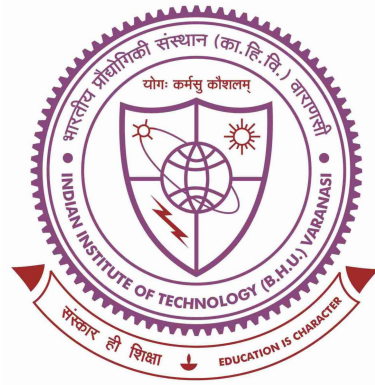


Out-of-time-order correlation in the quantum Ising Floquet spin system and magnonic crystals



Thesis submitted in partial fulfillment

for the Award of

DOCTOR OF PHILOSOPHY

in

PHYSICS

by

ROHIT KUMAR SHUKLA

Under the supervision of

Dr. Sunil Kumar Mishra

**DEPARTMENT OF PHYSICS
INDIAN INSTITUTE OF TECHNOLOGY
BANARAS HINDU UNIVERSITY
VARANASI - 221005**

ROLL NUMBER
17171002

YEAR OF SUBMISSION
2022

I would like to dedicate this thesis to my loving parents and amazing friends, whose support and motivation kept me going through the tough times.

Certificate

It is certified that the work contained in the thesis titled **Out-of-time-order correlation in the quantum Ising Floquet spin system and magnonic crystals** by **Mr. Rohit Kumar Shukla**, Roll Number **17171002**, has been carried out under my supervision, and this work has not been submitted elsewhere for a degree.

Signature: *Sunil Kumar Mishra*
23-12-2022

Dr. Sunil Kumar Mishra
Assistant Professor
Department of Physics
'77 (BHU), Varanasi-221

Supervisor
(Dr. Sunil Kumar Mishra)

Declaration

I, **Rohit Kumar Shukla**, certify that the work embodied in this thesis is my own bonafide work and carried out by me under the supervision of **Dr. Sunil Kumar Mishra** from July 2017 to December 2022 at the **Department of Physics**, Indian Institute of Technology (BHU), Varanasi. The matter embodied in this thesis has not been submitted for the award of any other degree. I declare that I have faithfully acknowledged and given credits to the research workers whenever and wherever their works have been cited in my work in this thesis. I further declare that I have not wilfully copied any others' work, paragraphs, text, data, results, etc., reported in journals, books, magazines, reports, dissertations, theses, etc., or available at websites and have not included them in this thesis and have not cited as my own work.

Date: 23/12/2022

Place: IIT(BHU), Varanasi

Rohit Shukla

23/12/2022

Signature of the Student

(Rohit Kumar Shukla)

Certificate by the Supervisor

It is certified that the above statement made by the student is correct to the best of my knowledge.

Signature:

Sunil Kumar Mishra
23-12-2022

Dr. Sunil Kumar Mishra

Assistant Professor
Department of Physics

IIT (BHU), Varanasi-221005

Signature of the Head of the Department

(Prof. Sandip Chatterjee)

HEAD/विभागाध्यक्ष

भौतिकी विभाग/Deptt. of Physics

सं.प्रौ.सं./कां.हि.वि.०/IIT (BHU)

वाराणसी/Varanasi-221005

Supervisor

(Dr. Sunil Kumar Mishra)

Sunil Kumar Mishra
Assistant Professor
Department of Physics
Indian Institute of Technology
(Banaras Hindu University)
Varanasi-221005

Sandip Chatterjee
23/12/22

Copyright Transfer Certificate

Title of the Thesis : Out-of-time-order correlation in the quantum Ising Floquet spin system and magnonic crystals

Name of the Student : Rohit Kumar Shukla

Copyright Transfer

The undersigned hereby assigns to the Indian Institute of Technology (Banaras Hindu University) Varanasi all rights under copyright that may exist in and for the above thesis submitted for the award of the **Doctor of Philosophy in Physics**.

Date: 23/12/2022

Rohit Shukla
23/12/2022
Signature of the Student

Place: IIT(BHU), Varanasi

(Rohit Kumar Shukla)

Note: However, the author may reproduce or authorize others to reproduce material extracted verbatim from the thesis or derivative of the thesis for author's personal use provided that the source and the Institute's copyright notice are indicated.

Acknowledgements

First of all, I would like to express my special thanks and gratitude towards my supervisor **Dr. Sunil Kumar Mishra** for introducing me to the field of quantum information and theoretical condensed matter physics, and for inspiring the incredible enhancement of my interest and understanding in this particular field of study. Without his outstanding supervision, unflinching support, unremitting discussions, and inestimable suggestions this journey would not have been possible. I thank him for giving me the opportunity to discuss each and every query related to the research work. His care and motivation for me were a strong driving force for the successful completion of my Ph. D.

I would further extend a special thanks towards my collaborators Dr. Arul Lakshminarayan, and Dr. Levan Chotorlishvili, who helped me throughout my research work. I have learned many things from them, for which I remain greatly indebted. Special thanks to my RPEC member Dr. Rajeev Singh, and Dr. Chandan Upadhyay for giving me valuable advice throughout this time, especially during the semester evaluation of the research progress.

I am very grateful to The Department of Physics for providing me with this wonderful opportunity, support, and facilities required for completing the project. I am thankful to all the technical, non-teaching, and office staff of the Department of Physics, IIT (BHU) for their continuous assistance and frequent co-operation at all the various stages of my Ph.D.

There are number of people I would like to acknowledge, without whose support, I could have never completed my Ph.D. work. These are Prashant Dixit, Digvijay, Prashant Pandey, Balveer, Vivek, Vaibhav, Abhishek, Alam, Suraj, Raj, Vipin, Gaurav, and Upendra, Deepak.

I feel short of words when expressing my thankfulness, gratitude, and indebtedness to my parents (Mr. Shankar Datta Shukla and Mrs. Baijanti Shukla), brother & sister-in-law

(Mr. Rahul Shukla & Mrs. Ansu Shukla), and sister (Miss. Stuti Shukla) for their unbiased love, blessings, inspiration, and support in countless ways.

Finally, I am highly obliged to the Almighty (Lord Shiva and Lord Sankat Mochan) for giving me patience and strength to make this endeavor a success.

Rohit Kumar Shukla

Abstract

In recent times out-of-time-order correlators (OTOC) have been established as a tool to understand butterfly effects, quantum information scrambling, and many-body localization. They can also be useful in determining different phases of quantum critical systems. OTOCs can identify the quantum chaos within a system undergoing time evolution; and therefore, they can distinguish between chaotic and regular dynamics. This motivates us to study OTOCs in integrable and nonintegrable periodically kicked quantum spin models. A periodically kicked quantum Ising spin system, known as the quantum Ising Floquet system, is a variant of the transverse Ising model. In place of constant transverse magnetic fields in the transverse Ising system, time-periodic fields are applied in the form of delta pulses in the quantum Ising Floquet spin system. It provides very interesting and peculiar dynamics separate from that of the transverse Ising system.

First, we explore the phase diagram of the Floquet transverse Ising model using the long-time average of OTOC as an order parameter. In the process, we present the exact analytical solution of the transverse magnetization OTOC using the Jordan-Wigner transformation. We also calculate the speed of correlation propagation and analyze the behavior of the revival time with the separation between the observables. To get the phase structure of the Floquet transverse Ising system, we use the longitudinal magnetization OTOC. We show the phase structure numerically in the transverse Ising Floquet system by using the long-time average of the longitudinal magnetization OTOC. In both the open and the closed chain systems, we find distinct phases, out of which two are paramagnetic (0-paramagnetic and π -paramagnetic), and two are ferromagnetic (0-ferromagnetic and π -ferromagnetic) as previously defined in the literature.

Next, we focus on different regimes of OTOC vs. time in the constant field transverse Floquet Ising system with and without longitudinal field. Three distinct regimes viz. char-

acteristic, dynamic, and saturation of OTOC vs. time, are analyzed carefully. In calculating OTOC, we take local spins in longitudinal and transverse directions as observables that are respectively local and non-local in terms of Jordan-Wigner fermions. We use the exact analytical solution of OTOC for the integrable model (without longitudinal field term) with transverse direction spins as observables and provide numerical solutions for other cases. OTOCs generated in both cases depart from unity at a kick equal to the separation between the observables when the local spins in the transverse direction and one additional kick is required when the local spins in the longitudinal direction. The number of kicks required to depart from unity depends on the separation between the observables and is independent of the Floquet period and system size. In the dynamic region, OTOCs show power-law growth in both models, the integrable (without longitudinal field) as well as the nonintegrable (with longitudinal field). The exponent of the power-law increases with increasing separation between the observables. Near the saturation region, OTOCs grow linearly with a very small rate.

Further, we calculate OTOCs using contiguous symmetric blocks of spins or random operators localized on these blocks as observables instead of localized spin observables. We find only the power-law growth of OTOC in integrable and nonintegrable regimes. In the non-integrable regime, beyond the scrambling time, there is an exponential saturation of the OTOC to values consistent with random matrix theory. This motivates the use of “pre-scrambled” random block operators as observables. A pure exponential saturation of OTOC in both integrable and nonintegrable systems is observed without a scrambling phase. Averaging over random observables from the Gaussian unitary ensemble, the OTOC is found to be the same as the operator entanglement entropy, whose exponential saturation has been observed in previous studies of such spin chains.

Finally, we utilize OTOCs as a quantifier for quantum information currents and propose a quantum information diode (QID) by exploiting the effect of nonreciprocal magnons

in a 2D Heisenberg spin system with Dzyloshinski Moriya interaction. QID is a device rectifying the amount of quantum information transmitted in opposite directions. We control the asymmetric left and right quantum information currents through an applied external electric field and quantify it through the left and right OTOC. To enhance the efficiency of the quantum information diode, we utilize a magnonic crystal. We excite magnons of different frequencies and let them propagate in opposite directions. Nonreciprocal magnons propagating in opposite directions have different dispersion relations. Magnons propagating in one direction match resonant conditions and scatter on gate magnons. Therefore, magnon flux in one direction is damped in the magnonic crystal. This fact leads to an asymmetric transport of quantum information in the quantum information diode. A quantum information diode can be fabricated from an yttrium iron garnet (YIG) film. This is an experimentally feasible concept and implies certain conditions: low temperature and small deviation from the equilibrium to exclude effects of phonons and magnon interactions. We show that rectification of the flow of quantum information can be controlled efficiently by an external electric field and magnetoelectric effects.

Overall, this thesis is focused on studying OTOC in the quantum Ising spin Floquet systems to describe the phase structure and dynamics of the systems. Additionally, it describes an application of OTOC as a quantifier of quantum information current in proposed QID based on magnonic crystals.

Table of contents

List of figures	xix
Nomenclature	xxvi
1 Introduction	1
1.1 Classical correlation	2
1.2 Quantum correlation	3
1.3 Temporal correlation	7
1.3.1 Time-ordered correlation	8
1.3.2 Out-of-time-order correlator	9
1.3.3 OTOC using position-dependent single spin observable	12
1.3.4 OTOC using block observables	14
1.4 Chaos	15
1.5 Chaotic Systems	15
1.5.1 Classical chaotic System	16
1.5.2 Quantum chaotic system	17
1.6 Spin-1/2	18
1.6.1 Spin-spin interaction	20
1.7 Heisenberg model	21
1.8 Ising Model	22

1.8.1	Boundary conditions	24
1.9	Transverse Ising model	25
1.10	Floquet transverse Ising model	25
1.10.1	Floquet map	26
1.10.2	Dzyaloshinskii–Moriya interaction (DMI)	28
1.10.3	2D square-lattice system with DMI interaction	29
1.11	Chaos in spin system	30
1.12	Magnons and spin wave	32
1.13	Magnonic crystal	33
1.13.1	Structure of magnonic crystal	33
1.14	Outline of the thesis	35
2	Out-of-time-order correlation and detection of phase structure in Floquet transverse Ising spin system	37
2.1	Introduction	37
2.2	Model	40
2.3	Out-of-time-order Correlation	40
2.4	Analytical calculation of TMOTOC	41
2.5	Speed for correlation propagation	43
2.6	Revival time	44
2.7	Phase Structure	46
2.7.1	Critical line with system size	50
2.8	Phase structure by frequencies of oscillations	51
2.9	Conclusion	52
3	Characteristic, dynamic and near saturation regions of Out-of-time-order correlation in Floquet Ising models	55

3.1	Introduction	55
3.2	Model	58
3.3	TMOTOC and LMOTOC	59
3.3.1	Analytical formula of TMOTOC	61
3.4	Results	62
3.4.1	TMOTOC in the integrable Floquet system	63
3.4.2	TMOTOC in the nonintegrable Floquet system	67
3.4.3	LMOTOC in the integrable Floquet system	69
3.4.4	LMOTOC in the nonintegrable Floquet system	71
3.5	Conclusion	73
4	Out-of-time-order correlation of the nonlocal block observables in Floquet Ising spin chain	75
4.1	Introduction	75
4.2	The spin model and background	78
4.2.1	The spin model	78
4.2.2	Out-of-time-order correlation and block operators	79
4.2.3	Average and asymptotic OTOC values	81
4.2.4	Nearest-neighbour spacing distribution	84
4.3	Constant field Floquet system	86
4.4	Special case	90
4.5	Conclusion	93
5	Quantum information diode based on the magnonic crystal	97
5.1	Introduction	97
5.2	Result	99
5.2.1	Proposed set-up for QID	99

5.2.2	Model	101
5.2.3	Out-of-time-order correlator	103
5.2.4	Rectification	106
5.3	Conclusions	107
6	Summary and Future Plans	109
6.1	Summary	109
6.2	Future plans	111
	References	113
Appendix A Out-of-time-order correlation and detection of phase structure in		
	Floquet transverse Ising spin system	129
A-I	Calculation of transverse magnetization OTOC	129
A-II	Calculation of Longitudinal Magnetization OTOC	134
Appendix B Characteristic, dynamic, and near saturation regions of Out-of-		
	time-order correlation in Floquet Ising models	135
B-I	Calculation of TMOTOC in the non-integrable Floquet system using ran- dom state	135
B-II	Time evolution of TMOTOC	136
B-III	Time evolution of LMOTOC	140
Appendix C Out-of-time-order correlators of nonlocal block-spin and random		
	observables in integrable and nonintegrable spin chains	143
C-I	Calculation of post-scrambling OTOC using random unitary operator . . .	143
C-I.1	Calculation of two-point correlation	144
C-I.2	Calculation of four point correlator	145

Appendix D	Quantum information diode based on a magnonic crystal	147
D-I	Diagonalization of Hamiltonian of 2D square lattice	147
D-II	Calculation of left and right out-of-time ordered correlation functions . .	149

List of figures

1.1	Contour of time folded that is showing the temporal ordered correlation of the observables $\hat{W}_1, \hat{W}_2, \hat{W}_3$, and \hat{W}_4 with times $t_1 < t_2 < t_3 < t_4$	8
1.2	Illustration of observable \hat{W} at time t and observable \hat{V} at initial time $t = 0$ which are not in time ordered manner. Arrows indicate the direction of the correlation defined for the operators along the time axis.	9
1.3	(Left) We consider a state $ \psi\rangle$ and apply operator $\hat{U}^\dagger \hat{W} \hat{U} \hat{V}$ and generate a state $ \phi(t)\rangle = \hat{U}^\dagger \hat{W} \hat{U} \hat{V} \psi\rangle$. (Right) We apply observable $\hat{V} \hat{U}^\dagger \hat{W} \hat{U}$ on state $ \psi\rangle$ and get state $ \xi(t)\rangle = \hat{V} \hat{U}^\dagger \hat{W} \hat{U} \psi\rangle$. Inner product of $ \xi(t)\rangle$ and $ \phi(t)\rangle$ is equal to $F(t)$	11
1.4	Schematics of single spin observables. One spin is considered as observable \hat{W} and another spin is considered as observable \hat{V}	13
1.5	Illustration of SBOs \hat{W} and \hat{V} represented by Eq. (1.24). The length of the chain is N that should be even to be divided into two halved subsystems \hat{W} and \hat{V}	14
1.6	Setup of Stern-Gerlach experiment.	19
1.7	Arrangement of spins at lattices in one, two, and three dimensions.	23
1.8	One-dimensional lattice configuration with (Left) periodic boundary condition and (Right) open boundary condition. Solid lines denote interaction.	25

1.9	Spin chain experience a periodic quench by non-commuting Hamiltonian functions \hat{H}_z and \hat{H}_x for durations τ_0 and τ_1 , respectively. The complete system is periodic with period $T = \tau_0 + \tau_1$	26
1.10	Local geometry to determine the DM vector's orientation.	29
1.11	Pictorial representation of magnonic transistor in which YIG film with grooves is deposited on GGG substrate. Three terminals of the microstrip antenna, such as the source, drain, and gate, are added to inject and measure the magnons.	35
2.1	Phase structure of the Floquet system with Floquet map given by Eq. (2.1). There are four distinct phases in the $\tau_0 - \tau_1$ parameter space. Two of these phases, the π ferromagnetic and the 0π paramagnetic, are phases which are unique to Floquet systems.	39
2.2	$F_z^{l,l}(n)$ for closed chain transverse Ising Floquet system of system size $N = 12$ by using the numerical calculations (solid line) and analytical expression of Eq. (2.7) (point). Here we take $\tau_0 = \tau_1 = \varepsilon$, where $\varepsilon = \frac{\pi}{28}$. .	43
2.3	Behaviour of (a) $F_z^{l,m}(n)$ and (b) $F_x^{l,m}(n)$ with number of kicks for different value of Δl . Here, the parameters are: $\tau_0 = \frac{\varepsilon}{2}$, $\tau_1 = \varepsilon$, and $N = 12$. In both figures (a) and (b), the inset shows the behavior of time of departure from unity ($t_{\Delta l}$) as a function of separation between the observables (Δl)	44
2.4	(a) Variation of the real part of (a) $F_x^{l,l}(n)$ and (b) $F_x^{l,l}(n)$ with number of Floquet periods for a fixed $\tau_0 = \varepsilon$ and $\tau_1 = \varepsilon, 2\varepsilon$ and 3ε in closed chain Floquet systems with system size $N=12$. Inset of the figure is the variation of $F_z^{l,l}(n)$ with the number of Floquet periods for a fixed $\tau_1 = \frac{\pi}{24}$ and $\tau_0 = \varepsilon, 2\varepsilon$ and 3ε in closed chain Floquet systems with system size $N=50$.	45

- 2.5 Variation of the real part of $F_x^{l,l}(n)$ with the number of Floquet periods for a fixed $\tau_0 = \varepsilon = \frac{\pi}{28}$ and multiple values of τ_1 in (a) closed and (b) open chain Floquet systems with system size $N=12$. The initial state is a direct product of the eigenstate of σ^x with eigenvalue $+1$. At $\tau_1 = 0$, $F_x^{l,l}(n)$ shows periodic oscillations about zero. As the value of τ_1 is increased, the $F_x^{l,l}(n)$ oscillates about greater non-zero values with lower amplitudes of oscillation and at $\tau_1 = \frac{\pi}{4}$, it saturates to the value 1. As increase constant value of τ_1 , $F_x^{l,l}(n)$ has same and different value as $\frac{\pi}{2} - \tau_1$ in closed and open chain respectively. 46
- 2.6 Plot of $\bar{F}_x^{l,l}(T)$ with τ_1 for values of τ_0 varying from 0 to $\frac{\pi}{4}$ in intervals of ε in the (a) closed and (b) open chain Floquet systems of system size $N = 10$ and $T = 10^4$. The variation of $\bar{F}_x^{l,l}(T)$ with τ_1 for $\pi/4 < \tau_0 < \pi/2$ is the same as that for $\frac{\pi}{2} - \tau_0$. This plot can be used to find the regions in the τ_0 and τ_1 parameter space that have $\bar{F}_x^{l,l}(T) > 0$ and $\bar{F}_x^{l,l}(T) = 0$ (Fig. 2.7). 48
- 2.7 Regions with $\bar{F}_x^{l,l}(T) > 0$ and $\bar{F}_x^{l,l}(T) = 0$ in the τ_0 and τ_1 parameter space with $T = 10^4$, for the (a)closed and (b) open chain Floquet systems of system size $N=6$ (Green), 8(Blue) and 10(Brown). As increasing system size, critical lines of both (a) and (b) tend towards diagonal critical lines. Hence, this suggests that the phase structure of the system would contain two ferromagnetic regions (where $\bar{F}_x^{l,l} > 0$) and two paramagnetic regions (where $\bar{F}_x^{l,l} = 0$). 49
- 2.8 Plot of the difference between finite size critical point and the infinite size critical point ($|\tau_{0c}(N) - \tau_{0c}(\infty)|$) of the phase structure of the periodic Floquet system as the function of system size (log-log plot). Black points are data points, and the red dashed line is the best fit yielding the slope $1/\nu = 0.8314 \pm 0.1122$ 51

2.9	Heat map of the logarithmic dominant frequencies of $F(n) - \overline{F}_x(T)$ in the discretized τ_0 - τ_1 parameter space for the (Left) closed and (Right) open Floquet system of system size $N = 10$ and with $T = 10^4$. The heat map shows logarithmically small values close to the transition lines shown in Fig. 2.7.	52
3.1	Schematic of the various regions of OTOC in a typical system.	62
3.2	Integrable transverse Ising Floquet system with $J_x = 1$ and $h_z = 1$ for $N = 18$. (a) The behavior of $TMOTOC$ with the number of kicks (n) by increasing the value of Floquet period from $\frac{7\varepsilon}{2}$ to $\frac{11\varepsilon}{2}$ differing by $\varepsilon/2$ with fixed $\Delta l = 6$ ($\varepsilon = \frac{\pi}{28}$). (b) $F_z^{l,m}$ with number of kicks by increasing Δl and fixed Floquet period $\tau = 6\varepsilon/2$. (c) $C_z^{l,m}$ with number of kicks (log – log) with increasing distances (Δl) between the spins at constant Floquet period $\tau = \frac{\varepsilon}{2}$. (d) Exponent of power-law with increasing distance between the spins. (e) $\Re[F_z^{l,m}]$ with number of kicks at different Δl	64
3.3	Integrable transverse Ising Floquet system with $J_x = 1$ and $h_z = 1$ for $N = 18$. Behaviour of $TMOTOC$ with number of kicks (n) by increasing Δl from 2 to 6 at different Floquet period (a) $\tau = \frac{2\varepsilon}{2}$, (b) $\tau = \frac{3\varepsilon}{2}$, (c) $\tau = \frac{4\varepsilon}{2}$, (d) $\tau = \frac{5\varepsilon}{2}$ and (e) $\tau = \frac{6\varepsilon}{2}$ ($\varepsilon = \frac{\pi}{28}$)	66
3.4	Non-integrable closed chain transverse Ising Floquet system with $J_x = 1$, $h_z = 1$, and $h_x = 1$ of size $N = 18$. (a) Behavior of $TMOTOC$ with number of kicks (n) by increasing value of Floquet period from $\frac{7\varepsilon}{2}$ to $\frac{11\varepsilon}{2}$ differing by $\frac{\varepsilon}{2}$ with fixed $\Delta l = 6$ ($\varepsilon = \frac{\pi}{28}$). (b) Initial region of $F_z^{l,m}$ with number of kicks with increasing distances between the spins (Δl) and fixed Floquet period $\tau = 6\varepsilon/2$. (c) $C_z^{l,m}$ with number of kicks (log – log) with increasing (Δl) at fixed $\tau = \frac{\varepsilon}{2}$. (d) Changing of power with Δl . (e) Saturation of $F_z^{l,m}$ with the number of kicks.	68

- 3.5 Integrable closed chain transverse Ising Floquet system with $J_x = 1$ and $h_z = 1$ of size $N = 18$. (a) Behaviour of *LMOTOC* with number of kicks (n) with increasing value of Floquet periods from $\frac{7\varepsilon}{2}$ to $\frac{11\varepsilon}{2}$ differing by $\frac{\varepsilon}{2}$ and $\Delta l = 6$ ($\varepsilon = \frac{\pi}{28}$). (b) $F_x^{l,m}(n)$ with number of kicks with increasing (Δl) and fixed Floquet period $\tau = 6\varepsilon/2$. (c) $C_x^{l,m}(n)$ with number of kicks ($\log - \log$) with increasing Δl at fixed $\frac{\varepsilon}{2}$. (d) Changing of power with Δl . (e) $F_x^{l,m}(n)$ with number of kicks at different Δl . Black line represents the exponential decreasing of maxima of saturation amplitude. 70
- 3.6 Non-integrable closed chain transverse Ising Floquet system with $J_x = 1$, $h_z = 1$, and $h_x = 1$ for $N = 18$. (a) *LMOTOC* with number of kicks (n) by increasing value of Floquet period from $\frac{7\varepsilon}{2}$ to $\frac{11\varepsilon}{2}$ differing by $\frac{\varepsilon}{2}$ with fixed $\Delta l = 6$ ($\varepsilon = \frac{\pi}{28}$). (b) $F_x^{l,m}(n)$ with increasing Δl from 6 to 6 and fixed period $\tau = \frac{6\varepsilon}{2}$. (c) $C_x^{l,m}(n)$ with number of kicks ($\log - \log$) by increasing Δl from 2 to 6 and fixed Floquet period $\tau = \frac{\varepsilon}{2}$. (d) Changing of power with Δl . (e) $F_x^{l,m}(n)$ with number of kicks at different Δl . Black line represents the exponential decrease of local maxima of saturating amplitude. 72
- 4.1 Schematics of SBOs defined in Eq. (4.5). Even N is considered and halved into subsystems W and V 80
- 4.2 Integrable $\hat{\mathcal{U}}_0$ system with parameters: $\tau = \frac{\pi}{18}$, $J_x = 1$, $h_x = 0$ and $h_z = 4$. (a) $C(n)/C(\infty)$ generated by SBOs vs. n for $N = 18$ ($\log - \log$). Line with points represents data from the numerical calculation, and the solid line is the polynomial fitting. Inset shows $1 - C(n)/C(\infty)$ vs. n ($\log - \text{linear}$). (b) $C(n)/C(\infty)$ vs. n for $N = 12$ and RBOs as observables. (c) $1 - C(n)/C(\infty)$ vs. n for $N = 12$ and RBOs as observables. Line with points is data generated numerically, and a solid line is the exponential fitting. (d) NNSD for $N = 12$. In all the cases, open boundary condition is considered. . . . 87

- 4.3 Nonintegrable $\hat{\mathcal{U}}_x$ system with parameters: $J_x = 1$, $h_x = 4$, $h_z = 4$ and $\tau = \frac{\pi}{18}$, $\frac{3\pi}{18}$. (a) Illustrates the $C(n)/C(\infty)$ by using the SBOs vs. n for $N = 18$ (log – log). Lines with points represent data from the numerical calculation, and solid lines are the polynomial fitting with exponent $b = 1.12$ at $\tau = \frac{\pi}{18}$ and $b = 1.74$ at $\tau = \frac{3\pi}{18}$. (b) $C(n)/C(\infty)$ by using the SBOs vs. n at different N for $\tau = \frac{3\pi}{18}$. (c) $1 - C(n)/C(\infty)$ vs. n (log – linear). Lines with points are data generated numerically, and solid lines are the exponential fitting. (d) Illustrates the OTOCs of RBOs vs. n for $N = 12$ (g) $1 - C(n)/C(\infty)$ vs. n (log – linear). Lines with points are data generated numerically, and solid lines are the exponential fitting. NNSD of the $\hat{\mathcal{U}}_x$ system at (f) $\tau = \frac{\pi}{18}$ and (g) $\tau = \frac{3\pi}{18}$ with $N = 12$. In all cases, an open boundary chain is considered. 89
- 4.4 (a) $C(n)/C(\infty)$ of SBOs vs. n in the $\hat{\mathcal{U}}_0$ system for $N = 18$. (b) log – log behavior of “a” in which lines with points represent data from the numerical calculation, and solid lines are the polynomial fitting. (c) $C(n)/C(\infty)$ of SBOs with n in the $\hat{\mathcal{U}}_x$ system for $N = 18$. (d) log – log behavior of “c” in which lines with points represent data from the numerical calculation, and solid lines are the polynomial fitting. (e) $C(n)/C(\infty)$ of RBOs vs. n in the $\hat{\mathcal{U}}_0$ and $\hat{\mathcal{U}}_x$ system for $N = 12$. (f) $1 - C(n)/C(\infty)$ vs. n for $N = 12$ (log – linear). Lines with points are data generated numerically, and solid lines are the exponential fitting. Other parameters: $J_x = 1$, $h_{0x} = 0/1$, $h_{0z} = 1$ and $\tau = \frac{\pi}{4}$. In all cases, an open boundary chain is considered. . . 91
- 4.5 Integrable $\hat{\mathcal{U}}_0$ system with parameters: $\tau = \frac{\pi}{4} - \varepsilon (= \frac{\pi}{50})$, $J_x = 1$, $h_x = 0$ and $h_z = 1$. (a) $C(n)/C(\infty)$ of SBOs vs. n in the $\hat{\mathcal{U}}_0$ system for $N = 18$. (b) log – log behavior of “a” in which lines with points represent data from the numerical calculation, and solid lines are the polynomial fitting. (c) NNSD of the $\hat{\mathcal{U}}_0$ system with $N = 12$ 93

- 4.6 (a) $C(n)/C(\infty)$ of SBOs vs. n in the $\hat{\mathcal{U}}_x$ system for $N = 12$ and 18. (b) log – log behavior of “a” in which lines with points represent data from the numerical calculation, and solid lines are the polynomial fitting. (c) $C(n)/C(\infty)$ of RBOs vs. n in the $\hat{\mathcal{U}}_0$ and $\hat{\mathcal{U}}_x$ system for $N = 12$. (d) $1 - C(n)/C(\infty)$ vs. n for $N = 12$ (log – linear). Lines with points are data generated numerically, and solid lines are the exponential fitting. (e) NNSD of the $\hat{\mathcal{U}}_x$ system for $N = 12$. Other parameters: $J_x = 1$, $h_x = 0/1$, $h_z = 1$ and $\tau = \frac{\pi}{4} - \varepsilon (= \frac{\pi}{50})$ 94
- 5.1 Illustration of a quantum information diode: A plane of an YIG film with grooves orthogonal to the direction of the propagation of quantum information. In the middle of the QID, we pump extra magnons to excite the system. A quantum excitation propagates toward the left, and the right ends asymmetrically. To describe the propagation process of quantum information, we introduce the left and right OTOC $C_L(t)$ and $C_R(t)$. Because the left-right inversion is equivalent to $D \rightarrow -D$ meaning $E_y \rightarrow -E_y$, we can invert the left and right OTOCs by switching the applied external electric field. 100
- 5.2 (a) Left-OTOC and (b) Right-OTOC with time t (in the units of $1/J$) for different distances $r_{1,2} = 10a, 20a$ and $30a$. (c) Right-OTOC with time for $r_{1,2} = 10a$ and suppression rates of the magnon current $\zeta = 0.8, 0.6$ and 0.4 . Parameters are $N = 1000$, $D = J_1 = 2J_2 = 1$. Periodic boundary conditions are considered. The values of the parameters: $m_0 = 1$ to N , $a = 10^{-3}$ and $a_0 = 1$ 105
- 5.3 Rectification coefficient R is plotted against DMI coefficient (D) for suppression rate $\zeta(D) \approx e^{-D/5}$. The parameters are $J_1 = 2J_2 = 1$, $N = 1000$, $r_{12} = 10a$, $a_0 = 1$ and $m_0 = 1$ to N 107

-
- B.1 Nonintegrable closed chain transverse Ising Floquet system with $J_x = 1$, $h_z = 1$, and $h_x = 1$ of size $N = 18$. **(a)** Behaviour of *TMOTOC* with number of kicks (n) by increasing Floquet period from $\frac{7\varepsilon}{2}$ to $\frac{11\varepsilon}{2}$ differing by $\frac{\varepsilon}{2}$ with fixed $\Delta l = 6$ ($\varepsilon = \frac{\pi}{28}$). **(b)** Initial region of $F_z^{l,m}$ with number of kicks and increasing distances between the spins (Δl) with fixed Floquet period $\tau = 6\varepsilon/2$. **(c)** $C_z^{l,m}$ with number of kicks ($\log - \log$) with increasing (Δl) at fixed $\tau = \frac{\varepsilon}{2}$ 137